Influence of anisotropy on thermal boundary conductance at solid interfaces

Patrick E. Hopkins,[1,2,*] Thomas Beechem,[2] John C. Duda,[1,2] Khalid Hattar,[2] Jon F. Ihlefeld,[2]
Mark A. Rodriguez,[2] and Edward S. Piekos[2]
[1]*Department of Mechanical and Aerospace Engineering, University of Virginia, Charlottesville, Virginia 22904, USA*
[2]*Sandia National Laboratories, Albuquerque, New Mexico 87123, USA*

(Received 15 July 2011; revised manuscript received 5 August 2011; published 6 September 2011)

We investigate the role of anisotropy on interfacial transport across solid interfaces by measuring the thermal boundary conductance from 100 to 500 K across Al/Si and Al/sapphire interfaces with different substrate orientations. The measured thermal boundary conductances show a dependency on substrate crystallographic orientation in the sapphire samples (trigonal conventional cell) but not in the silicon samples (diamond cubic conventional cell). The change in interface conductance in the sapphire samples is ascribed to anisotropy in the Brillouin zone along the principal directions defining the conventional cell. This leads to resultant phonon velocities in the direction of thermal transport that vary nearly 40% based on crystallographic direction.

DOI: 10.1103/PhysRevB.84.125408 PACS number(s): 68.35.−p, 66.70.−f, 66.90.+r, 61.80.Jh

I. INTRODUCTION

The thermal transport properties of nanosystems are strongly driven by the scattering rates at interfaces and boundaries. As characteristic lengths in nanosystems decrease, the influence of these material and geometric boundaries becomes more pronounced. In addition, decreasing sizes of nanosystems leads to increased anisotropy due to boundary scattering rates that vary based on direction. This anisotropy and its effects on thermal transport have been theoretically investigated in thin films[1,2] and superlattices,[3] for example. These works have shown that the boundary scattering rates differ in the in-plane versus cross-plane transport direction, leading to a directionally dependent thermal conductivity. The opposite situation of how material anisotropy affects boundary scattering rates and corresponding thermal boundary conductance, h_K, has been much less frequently studied. This thermal boundary conductance dependency on anisotropy and crystallographic orientation has been theoretically studied at interfaces comprised of graphite[4,5] and carbon nanotubes.[6] We are unaware of any experimental measurements showing an orientationally dependent thermal boundary conductance (i.e., how material anisotropy affects h_K). Clearly, greater insight into the mechanisms driving thermal transport across interfaces involving thermally anisotropic materials will not only have major implications for graphene-, graphite-, and carbon-nanotube-based devices, but will also elucidate the important thermal mechanisms intrinsic in other pertinent anisotropic systems, such as GaN, SiC, and Al_2O_3.

In response, in this paper we investigate the role of anisotropy on interfacial transport at Al/Si and Al/sapphire interfaces with different substrate orientations. We measure the thermal boundary conductance with time-domain thermoreflectance (TDTR). The measured thermal boundary conductance shows a dependency on substrate crystallographic orientation in the Al_2O_3 samples (trigonal conventional cell) but not in the silicon samples (diamond cubic conventional cell). The change in interface conductance in the sapphire samples is ascribed to anisotropy in the Brillouin zone along the principal directions defining the conventional cell. This leads to resultant phonon velocities in the direction of thermal transport that vary based on crystallographic direction more so than in the silicon cubic structures.

II. EXPERIMENTAL CONSIDERATIONS

To form the interfaces that are examined in this work, we evaporate Al films on Si (100) and (111) and Al_2O_3 (0001) (c plane) and $(11\bar{2}0)$ (a plane) substrates (we use hexagonal indices for sapphire throughout this paper). Silicon exhibits diamond cubic symmetry ($Fd\bar{3}m$, four axes of threefold symmetry), its Brillouin zone is approximately spherical, and the thermal conductivity of silicon is isotropic due to cubic symmetry. Sapphire has a trigonal conventional cell (with space group $R\bar{3}c$, one axis of threefold symmetry). Prior to aluminum evaporation, which was conducted at a base pressure of less than 2.0×10^{-7} Torr, the substrates were cleaned with a chemical rinse (acetone, methanol, and isopropyl alcohol). We evaporated ≈90 nm of aluminum on the substrates, but confirmed the exact thicknesses with picosecond ultrasonics[7] and profilometry. All of the Al films exhibited (111) out-of-plane orientation as confirmed with micro x-ray diffraction (μ-XRD); we also used μ-XRD to confirm the orientation of each of the substrates.

We measured h_K at the Al/Si and Al/Al_2O_3 interfaces with TDTR; typical experimental descriptions of TDTR and details of the thermal and lock-in analyses for thin-film systems are described elsewhere.[8–10] We modulated the pump path at 11 MHz and monitored the ratio of the real to imaginary signal of the probe beam ($-V_{in}/V_{out}$) locked into the pump frequency. We used a liquid-nitrogen cryostat with optical access to measure h_K from ∼100 to 500 K. For our analysis, we used bulk literature values for the heat capacity of each layer.[11] We estimated the reduced thermal conductivity of the Al transducer layer from electrical resistivity measurements on the Al film,[8] although over the time domain of interest in this study, the TDTR analysis was minimally sensitive to the reduction in thermal conductivity of the Al film. We used h_K in our model as the free parameter and adjusted its value to match the data. We adjusted the thermal conductivity of the substrate to improve the fit of the model to the data. Note that the thermal conductivity and thermal boundary conductance

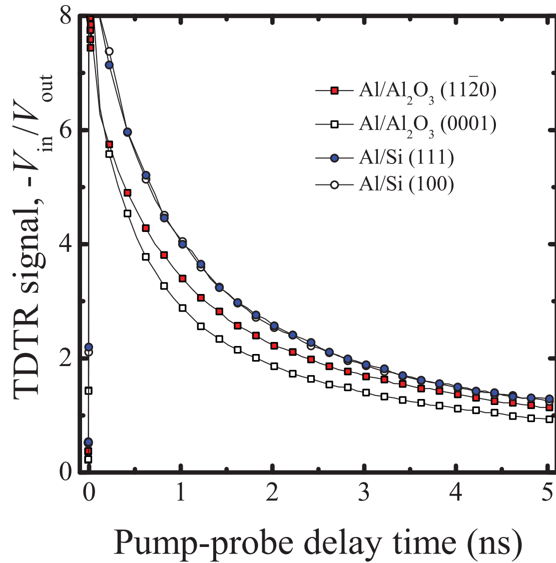

FIG. 1. (Color online) Room-temperature TDTR data on the Al/Si and Al/Al_2O_3 interfaces with different substrate orientations. The TDTR data on the Si (100) and (111) interfaces were nearly identical, and appear nearly perfectly overlapped. There is a clear difference between the TDTR data taken on the two differently oriented sapphire samples that is caused by the different thermal boundary conductances between the Al/Al_2O_3 (0001) and (11$\bar{2}$0) interfaces.

can be determined independently for these film/substrate systems.

III. RESULTS

Figure 1 shows examples of TDTR data taken at 294 K on the Al/Si and Al/Al_2O_3 interfaces with different orientations. The TDTR data on the silicon (100) and (111) interfaces were nearly identical, and appear nearly perfectly overlapped in Fig. 1. There is a clear difference between the TDTR data taken on the two differently oriented sapphire samples that is caused by the different thermal boundary conductances between the Al/Al_2O_3 (0001) and (11$\bar{2}$0) interfaces. We note that h_K can depend on differing structures and qualities of each individual interface.[12–17] To gain confidence that our observations of h_K in these systems are not attributed to differences in interfacial quality that could arise from sample variations, we test three different samples from different wafers for each interface. We take three TDTR data sets on each sample; our reported data in this work represent the average of the subsequent nine data sets on each interface with standard deviations among the nine sets represented by the error bars.

Figure 2 shows the measured thermal boundary conductance on the four types of interfaces examined in this study as a function of temperature. For comparison, we also show measurements from Costescu *et al.*,[18] who used TDTR to measure h_K across TiN/MgO interfaces for differently oriented MgO substrates. TiN and MgO exhibit cubic symmetry, and there is no discernible difference in the reported h_K across the TiN/MgO interfaces over the measured temperature range, similar to the Al/Si interfaces. The Al/Al_2O_3 interfaces, however, show a clear difference in thermal boundary conductance.

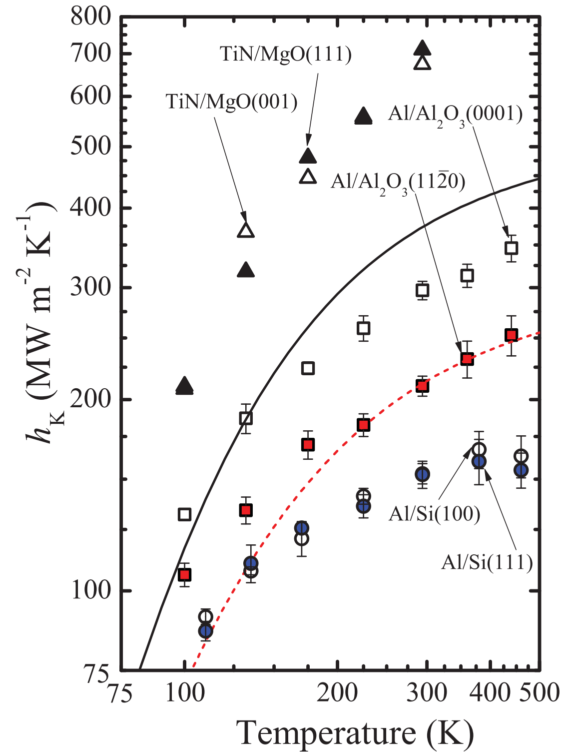

FIG. 2. (Color online) Measured thermal boundary conductance on the four types of interfaces examined in this study as a function of temperature. For comparison, we also show the measured h_K across TiN/MgO interfaces for differently oriented MgO substrates.[18] Silicon exhibits cubic symmetry, and there is no discernible difference in the reported h_K across the Al/Si interfaces over the measured temperature range, similar to the TiN/MgO interfaces. The Al/Al_2O_3 samples exhibit a clear dependence on sapphire substrate orientation. We model h_K across the Al/Al_2O_3 interfaces with the model discussed in this work that is based on the DMM but accounts for anisotropy by considering a cylindrically symmetric Brillouin zone. The black, solid line represents our DMM calculations for the Al/Al_2O_3 (0001) interfaces and the red, dashed line represents our DMM calculations for the Al/Al_2O_3 (11$\bar{2}$0) interfaces. The model captures the substrate orientation dependency in the experimental data well, along with exhibiting good agreement in the measured values.

As discussed in much greater detail below, we ascribe this to the differently oriented sapphire substrates exhibiting different net phonon velocities in the direction normal to the interface, which is much more pronounced in structures without cubic symmetry.

We do not observe any conclusive degree of anisotropy in the fitted thermal conductivities over the entire temperature range for both the silicon and sapphire samples. In general, we observe a substantial departure from the bulk, literature values for the substrate thermal conductivities at temperatures below about 200 K, where our values at room temperature and above agree to within 20% of those in the literature.[19] For example, our average values for the thermal conductivities of the silicon substrates at 110 K and the sapphire substrates at 100 K are 400 and 220 $\mathrm{W\,m^{-1}\,K^{-1}}$, respectively. These values are lower than the previously reported values for the thermal conductivities of bulk, single-crystal silicon and sapphire at these temperatures (742 and 350–500 $\mathrm{W\,m^{-1}\,K^{-1}}$, respectively).[19] The reason for

this discrepancy could be due to several factors having to do primarily with the near-surface measurement aspect of TDTR. Since TDTR is a near-surface measurement technique, any subsurface damage or impurities in the substrate could give rise to an apparent reduction in thermal conductivity.[20] This would explain why the values at room temperature are slightly lower than bulk and why there is a larger deviation from the bulk values at low temperatures. Since the long-wavelength phonons, which are more populous at low temperatures, would scatter with the near-surface defected region more readily, this would lead to a larger difference between the measured thermal conductivity and the literature values. The other possible explanation for the discrepancy in thermal conductivities at low temperatures could be the frequency-dependent thermal conductivity idea pioneered by Koh and Cahill.[21] In their work, they used TDTR to show that at very high modulation frequencies (similar to the modulation frequency used in this work), the thermal penetration depth induced from the TDTR pump-beam modulation can be less than the mean free path of the long-wavelength phonons in the substrate. In this case, TDTR would not "capture" all of the phonons in the measurement volume, and the apparent thermal conductivity would be lower than that of bulk. Although Koh and Cahill only observed this effect in semiconductor alloys, given the large zone-center phonon velocities in both silicon and sapphire, this phenomenon could be observed in these substrates at lower temperature where mean free paths are long compared to the thermal penetration depth. As the focus of this paper remains on the thermal boundary conductance and its functionality on substrate orientation and not on the thermal conductivity of the substrate, a more in-depth study and analysis of the thermal conductivity of the substrate is not pursued here.

IV. DISCUSSION AND ANALYSIS

To gain insight into the experimental results, we turn to the diffuse mismatch model (DMM) to predict the thermal boundary conductance.[22] In its most general form, the phonon flux in some material approaching an interface is given by

$$q = \frac{1}{8\pi^3}\sum_j \int_{k_x}\int_{k_y}\int_{k_z} \hbar\omega f v_{g\perp,j}\, dk_x dk_y dk_z, \quad (1)$$

where ω is the phonon angular frequency, k is the wave vector, f is the phonon distribution function, which, for this work, we assume to be the Bose-Einstein distribution function, $v_{g\perp}$ is the phonon group velocity perpendicular to the interface, and j refers to the phonon polarization. The group velocity represents the phonon velocity in the direction of the applied thermal gradient, and $v_{g\perp,j} = v_{g,j}\cos\theta$, where θ represents the polar angle between the wave vector of the incident phonon and the normal to the interface. In the diffusive limit, $\zeta^{1\to 2} = 1 - \zeta^{2\to 1}$. Applying the principle of detailed balance,[23] the transmission coefficient becomes[24]

$$\zeta_{1\to 2} = \frac{q_2}{q_1 + q_2}, \quad (2)$$

where, assuming elastic scattering, we only consider frequencies in the fluxes up to the maximum cutoff frequency of the lower-frequency solid (e.g., for the Al/Al_2O_3 interface, we only consider frequencies less than the cutoff frequency of Al in the "side 2" sapphire flux). In Eq. (2), the subscripts indicate calculations of Eq. (1) using the material properties from side 1 or 2. From Eq. (1), and using the fact that $h_K = \partial q/\partial T$ in the limit of an infinitesimally small temperature drop (i.e., what is assumed in detailed balance), the thermal boundary conductance from material 1 to material 2 as predicted by the DMM is given by

$$h_K = \frac{1}{8\pi^3}\sum_j \int_{k_x}\int_{k_y}\int_{k_z} \hbar\omega \frac{\partial f}{\partial T} v_{g,1,j}\cos\theta\,\zeta_{1\to 2}\, dk_x dk_y dk_z. \quad (3)$$

In cubic structures, a spherical shape can be assumed to approximate the shape of the Brillouin zone. Exploiting spherical symmetry, the volume element from Eq. (1) $dk_x dk_y dk_z \to k^2 dk \sin\theta d\theta d\phi$, where ϕ is the azimuth, so Eq. (1) becomes

$$q = \frac{1}{8\pi^3}\sum_j \int_0^{2\pi}\int_0^{\pi/2}\int_k \hbar\omega f v_{g,j} k^2 \sin\theta\cos\theta\, dk d\theta d\phi, \quad (4)$$

which is the isotropic assumption in the DMM that is discussed elsewhere.[24,25] Note that in cubic crystals, $v_{g,x} = v_{g,y} = v_{g,z}$ [e.g., in Si, the dispersions along the (100), (010), and (001) directions are identical]. Assuming a diffusively scattering flux at the interface, the integration over polar and azimuth angles can be executed without loss of generality. Therefore, the flux that is scattered diffusively at the interface assuming an isotropic, spherical Brillouin zone becomes

$$q = \frac{1}{8\pi^2}\sum_j \int_k \hbar\omega f v_{g,j} k^2\, dk. \quad (5)$$

With this isotropic Brillouin zone assumption, the thermal boundary conductance becomes

$$h_K = \frac{1}{8\pi^2}\sum_j \int_k \hbar\omega \frac{\partial f}{\partial T} v_{g,1,j}\zeta_{1\to 2} k^2\, dk. \quad (6)$$

In materials with noncubic lattice structures, spherical symmetry cannot be assumed in the Brillouin zone. For example, graphite and Al_2O_3 have oblong Brillouin zones due to their rhombohedral shaped primitive cells. Therefore, the Brillouin zone can be approximated by a cylindrical or ellipsoidal shape as opposed to the spherical shape used to approximate cubic structures. In this work, we adopt the convention of approximating the Al_2O_3 Brillouin zone as cylindrical, which follows from previous modeling of thermal transport at graphite and carbon nanotube interfaces.[6] Assuming cylindrical symmetry, the volume element from Eq. (1) $dk_x dk_y dk_z \to k_r dk_r dk_z d\theta$, and Eq. (1) becomes

$$q = \frac{1}{8\pi^3}\sum_j \int_{-\pi/2}^{\pi/2}\int_{k_z}\int_{k_r} \hbar\omega f v_{g,j} k_r \cos\theta\, dk_r dk_z d\theta, \quad (7)$$

where $k_r^2 = k_x^2 + k_y^2$. Therefore, the flux that is scattered diffusively at the interface assuming a cylindrical Brillouin

zone becomes

$$q = \frac{1}{4\pi^3} \sum_j \int_{k_z} \int_{k_r} \hbar\omega f v_{g,j} k_r \, dk_r dk_z. \quad (8)$$

To model h_K in the Al/Al_2O_3 samples, we determine h_K by using the flux from side 1 to side 2 given by Eq. (6) and the transmission using Eq. (2) with Eqs. (5) and (8) for Al and Al_2O_3, respectively. Therefore, the only information needed for calculation of h_K is the dispersion (and group velocity derived from the dispersion). Instead of making a Debye[26] or sine-type[27] assumption regarding the phonon dispersion, we fit a polynomial to the dispersion predicted via previously published lattice-dynamics simulations in the direction of high symmetry that most accurately represents the correct size of the Brillouin zone.[25] In Al, we choose the (100) direction from Gilat and Nicklow.[28] In sapphire, we consider k_r as the $(11\bar{2}0)$ orientation represented by the $\Gamma \rightarrow D$ direction and k_z as the (0001) orientation represented by the $\Gamma \rightarrow Z$ direction. We use the phonon dispersions in these directions of high symmetry by Heid *et al.*[29] Since the two orientations of the sapphire substrates studied in this work are orthogonal, when predicting h_K in a (0001) oriented sapphire substrate we only use the velocities from the $\Gamma \rightarrow Z$ direction to describe the phonon propagation and vice versa for the $(11\bar{2}0)$ direction. The predictions for our Al/Al_2O_3 DMM assuming a sapphire substrate orientation of either (0001) or $(11\bar{2}0)$ agree well with, and show a very similar dependency on orientation to, our experimental measurements.

To evaluate the validity of our assumptions in our DMM calculations, we calculate h_K with the DMM using a Debye assumption and assuming either a spherical Brillouin zone [Eq. (5)] or a cylindrical Brillouin zone [Eq. (8)] in the sapphire. For the Debye velocities, we use the average speeds of sound reported by Swartz and Pohl[22] for the isotropic calculations. For the cylindrically symmetric Debye DMM calculations, we use the zone-center velocities in the $\Gamma \rightarrow Z$ and $\Gamma \rightarrow D$ directions taken from the lattice dynamics results by Heid *et al.*[29] Results of these two Debye-based DMM calculations are shown in Fig. 3 along with the data and the model using a realistic dispersion for sapphire from Fig. 2. The isotropic Debye assumption does not capture the temperature trends in the data, along with the fact that assuming an isotropic medium, there is no way to show any dependency on crystallographic orientation while still consistently taking into account the correct number of phonon modes. The cylindrically symmetric Debye calculations only show a very weak dependency with sapphire orientation, and do not explain the experimental data. The reason that our DMM calculations using a realistic dispersion show much better agreement than the Debye approaches is due to the multiple phonon modes that have higher frequencies than the lower-frequency acoustic modes assumed in the Debye calculations. These higher-energy modes have significantly reduced group velocities from the zone-center acoustic modes, and these velocities are significantly different in the different crystallographic directions. This leads to the majority of the difference in the measured h_K in the two different sapphire samples. This demonstrates the importance of properly accounting for the phonon dispersion in the materials comprising the interface

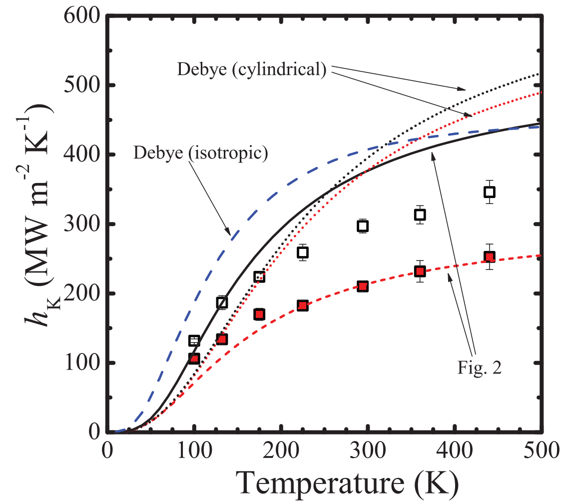

FIG. 3. (Color online) Al/sapphire DMM calculations assuming either a Debye assumption with a spherical Brillouin zone (blue, dashed line), a Debye assumption with a cylindrical Brillouin zone (black and red dotted lines), or the realistic dispersion, replotted from the model used in Fig. 2 along with the measured data in the (0001) or $(11\bar{2}0)$ sapphire samples. Although the cylindrical assumption with a Debye dispersion does exhibit some degree of anisotropy in the predicted h_K, it does not capture the difference observed experimentally. Using realistic dispersions in the different directions captures the experimental data much better than the Debye assumptions.

when predicting h_K, especially in materials with complex unit cells and nonspherical Brillouin zones.

To explore the origin of this orientationally dependent thermal boundary conductance, we calculate the following quantity:

$$\langle v_{r/z} \rangle = \sum_j \left(\frac{\int_{k_{r/z}} f v_{g,r/z,j}(k) \, dk_{r/z}}{\Delta k_{r/z,j}} \right), \quad (9)$$

which we define as a Brillouin zone averaged velocity. In Eq. (9), f is the Bose-Einstein distribution function, j is an index that refers to the phonon polarization, k is the wave vector, v_g is the phonon group velocity, which is a function of k, and the subscripts r and z represent the properties of the $(11\bar{2}0)$ and (0001) directions, respectively, for sapphire, and the (100) and (111) directions, respectively, for silicon. For calculations of Eq. (9), we only consider frequencies up to the maximum phonon frequency of aluminum, which parallels a typically employed assumption of only two-phonon elastic-scattering events participating in thermal boundary conductance.[30] The denominator, Δk, represents the width of the Brillouin zone over which the phonon velocities of a given branch are averaged, which is different for each orientation, and can be different for each branch in a given orientation since we only include phonons with frequencies less than the maximum frequency in Al in these calculations. For the phonon dispersion, we fit a polynomial to the dispersion predicted via previously published lattice-dynamics simulations in the direction of high symmetry representing the crystallographic direction of interest.[25] In sapphire, we consider k_r as the $(11\bar{2}0)$ orientation represented by the $\Gamma \rightarrow D$ direction and k_z as the

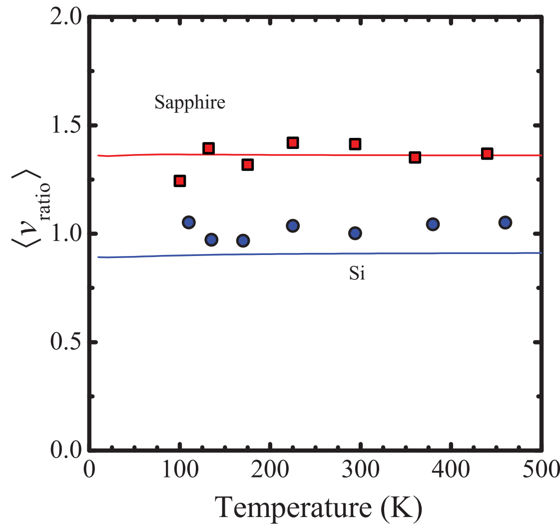

FIG. 4. (Color online) Equation (10) calculated for the two crystallographic directions of sapphire and silicon compared to the ratio of the measured h_K shown in Fig. 2. The excellent agreement indicates that the differences in velocities in the different crystallographic directions of sapphire lead to the differences in h_K.

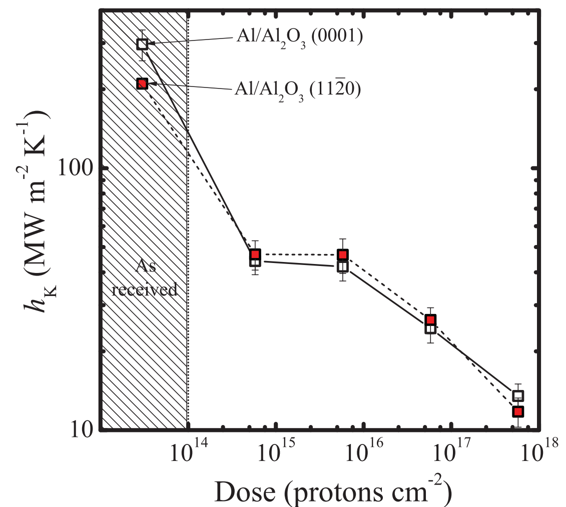

FIG. 5. (Color online) Thermal boundary conductance at the Al/Al_2O_3 (0001) and (11$\bar{2}$0) interfaces as a function of proton dose. We ascribe the sharp decrease in h_K from the as-received samples to the lowest ion-implanted samples due to bond breaking from the proton irradiation, and the dependence of h_K on proton dose is related to the atomic displacement and near-surface morphology.[33] This disorder and local amorphization lead to an isotropic thermal boundary conductance.

(0001) orientation represented by the $\Gamma \rightarrow Z$ direction. We use the phonon dispersions in these directions of high symmetry by Heid *et al.*[29] For silicon, we arbitrarily label k_r as the (111) direction and k_z as the (100) direction and use the dispersion of silicon reported by Weber for calculations of Eq. (9) (Ref. 31).

The ratio of

$$\langle v_{\mathrm{ratio}} \rangle = \frac{\langle v_z \rangle}{\langle v_r \rangle} \tag{10}$$

is shown in Fig. 4 along with the ratio of the measured h_K on both the sapphire and silicon samples. The agreement between the quantity calculated via Eq. (10) and the ratio of the measured data indicates that the differences in velocities in the different crystallographic directions of sapphire lead to the majority of the differences in the measured thermal boundary conductance. Note that the elastic constants in the different directions of sapphire are very similar, and cannot fully describe our anisotropic observation; however, the high-frequency, highly dispersive modes in the Al_2O_3 are drastically different and give rise to the observed anisotropy in the thermal boundary conductance, as we have previously discussed. We note that Eq. (10) predicts a very slight anisotropy in the average phonon velocities in the differently oriented silicon samples, which, based on our reasoning, should manifest itself as different thermal boundary conductances in the Al/Si(100) and Al/Si(111) samples. We do not observe any significant anisotropy in the two differently oriented Al/Si interfaces, however. As the predicted difference in average group velocities is less than 10%, we do not expect to be able to resolve difference with TDTR.[32] However, it is also important to note that in our calculations of Eqs. (9) and (10) (and our DMM calculations, for that matter), we only ratio the velocities in a single crystallographic direction of high symmetry. In reality, there will be phonons at various angles to the direction of high symmetry that will contribute some portion to phonon heat flow, which could reduce the magnitude of the predicted anisotropy, especially in cubic structures where the (100) and (111) are not orthogonal.

V. ION-IRRADIATED AL/SAPPHIRE INTERFACES

Since our results and analysis indicate that the velocities of the dispersive modes in the different crystallographic directions of sapphire are the origin of the anisotropic thermal boundary conductance, a change in the velocities of these dispersive modes near the interface should change the degree of anisotropy. Specifically, if the crystallographic symmetry is destroyed via damage or amorphizing the Al_2O_3 near the Al/Al_2O_3 boundary, we presumably can reduce the degree of observed anisotropy. To test this, we implanted Al_2O_3 (0001) and (11$\bar{2}$0) substrates with 300 keV protons at 1.2 μA using a 400 keV implanter at the Ion Beam Laboratory at Sandia National Laboratories in Albuquerque, NM. We implanted the sapphire substrate prior to Al film deposition. Details of the specific implantation parameters are described elsewhere.[33] We then used TDTR to measure the thermal boundary conductance as a function of proton dose, as shown in Fig. 5. As we have discussed in detail in our previous work,[33] the proton implantation leads to a large change in the crystalline properties of the sapphire near the surface, but the relative effects on the thermal properties of the substrate region in the TDTR thermal penetration depth is much less severe. Much of this has to do with the fact that the end of the range of protons in this irradiation procedure is nearly 1.7 μm from the sapphire surface, where the thermal penetration depth of sapphire at room temperature is only 500–600 nm at a pump modulation frequency of 11 MHz. The majority of the crystal damage occurs at the end of the range. However, very near the sapphire surface, swelling and crystalline damage occurs due to relaxation processes

propagating to the surface from the end of the range. After irradiation, when the samples are capped with the Al film for TDTR measurements, the majority of the change due to the proton implantation is therefore due to the Al/sapphire thermal boundary conductance (due to the very near-surface morphology) and not the reduction in thermal conductivity since the measurements do not probe deep enough to reveal the end-of-range damage. This is an important consideration since the substrate thermal conductivity in the probed region does not decrease substantially so that the measurement is still extremely sensitive to the Al/sapphire thermal boundary conductance. This aspect of proton implantation and relative reduction in thermal boundary conductance and substrate thermal conductivity is discussed in much greater detail in our previous work.[33]

Upon proton bombardment, h_K loses its dependence on the crystallographic direction; that is, the anisotropic nature of h_K at the Al/sapphire interface is destroyed. We attribute this to subsurface disorder in sapphire near the interface, such that amorphization destroys the crystallographic anisotropy in sapphire, thereby leading to isotropic phonon velocities and subsequent isotropy in h_K. Given this, we cannot preclude the possibility that there could be some degree of disorder among the various wafers used to form the Al/Si interfaces examined in this study, thereby resulting in the nearly identical measurements of h_K at the (100) and (111) interfaces. Our Al/Si h_K measurements in fact do exhibit trends similar to our previous measurements of Al/Si h_K with a few nanometers of roughness at the Si surface.[17] However, even at perfect Al/Si interfaces with no roughness, any slight anisotropy would most likely not be observable due to the uncertainties in TDTR measurements.[32]

VI. SUMMARY

In summary, we have investigated the role of anisotropy on interfacial transport at Al/Si and Al/sapphire interfaces with different substrate orientations. The measured thermal boundary conductance shows a dependency on substrate crystallographic orientation in the Al_2O_3 samples (trigonal) but not in the Si samples (cubic). The change in interface conductance in the sapphire samples is ascribed to the resultant phonon velocities in the direction of thermal transport that vary based on crystallographic direction. This is verified with diffuse mismatch model calculations and calculations of the average phonon velocity in each crystallographic direction. Furthermore, we find that ion irradiation of the sapphire substrates destroys the anisotropic effects on thermal boundary conductance.

ACKNOWLEDGMENTS

We are grateful for funding from the LDRD program office through the Sandia National Laboratories. P.E.H. is grateful for funding through the Harry S. Truman Fellowship Program and Sandia. J.C.D. is appreciative of funding through the National Science Foundation Graduate Research Fellowship Program and the Student Internship Program at Sandia. We are grateful for the assistance of James Griego during the μ-XRD measurements. This work was performed, in part, at the Center for Integrated Nanotechnologies, a US Department of Energy, Office of Basic Energy Sciences user facility. Sandia National Laboratories is a multiprogram laboratory managed and operated by Sandia Corporation, a wholly owned subsidiary of Lockheed Martin Corporation, for the US Department of Energy's National Nuclear Security Administration under Contract No. DEAC04-94AL85000.

*phopkins@virginia.edu

[1] J. E. Turney, A. J. H. McGaughey, and C. H. Amon, J. Appl. Phys. **107**, 024317 (2010).

[2] D. P. Sellan, J. E. Turney, A. J. H. McGaughey, and C. H. Amon, J. Appl. Phys. **108**, 113524 (2010).

[3] G. Chen, Phys. Rev. B **57**, 14958 (1998).

[4] J. C. Duda, J. L. Smoyer, P. M. Norris, and P. E. Hopkins, Appl. Phys. Lett. **95**, 031912 (2009).

[5] J. C. Duda, P. E. Hopkins, T. E. Beechem, J. L. Smoyer, and P. M. Norris, Superlattices Microstruct. **47**, 550 (2010).

[6] R. S. Prasher, Phys. Rev. B **77**, 075424 (2008).

[7] C. Thomsen, J. Strait, Z. Vardeny, H. J. Maris, J. Tauc, and J. J. Hauser, Phys. Rev. Lett. **53**, 989 (1984).

[8] P. E. Hopkins, J. R. Serrano, L. M. Phinney, S. P. Kearney, T. W. Grasser, and C. T. Harris, J. Heat Transfer **132**, 081302 (2010).

[9] D. G. Cahill, Rev. Sci. Instrum. **75**, 5119 (2004).

[10] A. J. Schmidt, X. Chen, and G. Chen, Rev. Sci. Instrum. **79**, 114902 (2008).

[11] F. Incropera and D. P. DeWitt, *Fundamentals of Heat and Mass Transfer*, 4th ed. (Wiley, New York, 1996).

[12] E. T. Swartz and R. O. Pohl, Appl. Phys. Lett. **51**, 2200 (1987).

[13] P. E. Hopkins, P. M. Norris, R. J. Stevens, T. Beechem, and S. Graham, J. Heat Transf. **130**, 062402 (2008).

[14] P. E. Hopkins, L. M. Phinney, J. R. Serrano, and T. E. Beechem, Phys. Rev. B **82**, 085307 (2010).

[15] P. E. Hopkins, J. C. Duda, S. P. Clark, C. P. Hains, T. J. Rotter, L. M. Phinney, and G. Balakrishnan, Appl. Phys. Lett. **98**, 161913 (2011).

[16] P. E. Hopkins and P. M. Norris, Appl. Phys. Lett. **89**, 131909 (2006).

[17] P. E. Hopkins, J. C. Duda, C. W. Petz, and J. A. Floro, Phys. Rev. B **84**, 035438 (2011).

[18] R. M. Costescu, M. A. Wall, and D. G. Cahill, Phys. Rev. B **67**, 054302 (2003).

[19] *Thermal Conductivity-Nonmetallic Solids*, Thermophysical Properties of Matter Vol. 2 (IFI/Plenum, New York, 1970).

[20] R. J. Stoner and H. J. Maris, Phys. Rev. B **48**, 16373 (1993).

[21] D. G. Cahill and R. O. Pohl, Phys. Rev. B **35**, 4067 (1987).

[22] E. T. Swartz and R. O. Pohl, Rev. Mod. Phys. **61**, 605 (1989).

[23] W. G. Vincenti and C. H. Kruger, *Introduction to Physical Gas Dynamics* (Krieger, Malabar, FL, 2002).

[24] J. C. Duda, P. E. Hopkins, J. L. Smoyer, M. L. Bauer, T. S. English, C. B. Saltonstall, and P. M. Norris, Nanoscale Microscale Thermophys. Eng. **14**, 21 (2010).

[25] J. C. Duda, T. Beechem, J. L. Smoyer, P. M. Norris, and P. E. Hopkins, J. Appl. Phys. **108**, 073515 (2010).
[26] N. W. Ashcroft and N. D. Mermin, *Solid State Physics* (Saunders College, Fort Worth, TX, 1976).
[27] G. Chen, J. Heat Transf. **119**, 220 (1997).
[28] G. Gilat and R. M. Nicklow, Phys. Rev. **143**, 487 (1966).
[29] R. Heid, D. Strauch, and K. P. Bohnen, Phys. Rev. B **61**, 8625 (2000).
[30] P. E. Hopkins, J. Appl. Phys. **106**, 013528 (2009).
[31] W. Weber, Phys. Rev. B **15**, 4789 (1977).
[32] Y. K. Koh, S. L. Singer, W. Kim, J. M. O. Zide, H. Lu, D. G. Cahill, A. Majumdar, and A. C. Gossard, J. Appl. Phys. **105**, 054303 (2009).
[33] P. E. Hopkins, K. Hattar, T. Beechem, J. F. Ihlefeld, D. L. Medlin, and E. S. Piekos, Appl. Phys. Lett. **98**, 231901 (2011).